

Temperature control of an SThM micro-probe with an heat source estimator and a lock-in measurement

M. Lenczner¹, B. Yang¹, S. Cogan¹, S. Domas¹, D. Ke¹, R. Couturier¹, D. Renault², B. Koehler³, P. Janus⁴

¹FEMTO-ST, UFC-CNRS-UTBM-ENSMM,
26 chemin de l'Épitaphe, 25030 Besançon Cedex, France
²ODESIM, 1 vallon fleuri, 25660 Morre, France

³Fraunhofer-Institut für Keramische Technologien und Systeme (IKTS), Maria Reiche Str. 2, 01109 Dresden, Germany

⁴Instytut Technologii Elektronowej, al. Lotnikow 32/46, 02-669 Warsaw, Poland

Email: {michel.lenczner, bin.yang, scott.cogan, stephane.domas, du.ke, raphael.couturier }@femto-st.fr,
david.renault@odesim.com, Bernd.Koehler@ikts-md.fraunhofer.de, janus@ite.waw.pl

Abstract

In view of qualitative temperature measurement by scanning thermal microscopy, we introduce a model-based control law for a new microfabricated probe. The underlying model is the time-space two-scale electro-thermal model presented in [15], since it has the power to represent transients of harmonic modulations. The control method accounts for an estimation of the heat source in the sample and for the delay in the lock-in filter based observation. Experiment-based model calibration is a prerequisite and is discussed in detail.

Keywords. *Scanning Thermal Microscopy, Model Parameter Calibration, Multiscale Model, Temperature Control, Control with Delay in Observation, Lock-in Amplifier, Source Estimation*

1. Introduction

The Scanning Thermal Microscopy (SThM) is a kind of scanning probe microscopy for mapping thermal transport and temperature on surfaces. During the last twenty years, systems combining an AFM cantilever with a thermoresistive three dimensional tip have been developed [16, 6, 17, 14]. Here, we refer especially to this developed by Gotszalk and his coworkers in [18, 9, 8]. Recently, Janus and his colleagues have proposed a novel design [11] expecting quantitative temperature measurement in the range of 1K with a resolution of few tenths of nanometers. Main novelty of proposed solution is the deflection measurement technique based on piezoresistive deflection sensing. This type of detection allows for removing laser spot that, according to authors previous works, causes unwanted heat at tip's area [10]. Moreover, this type of probe can be easier integrated with nanomanipulator arm or in small AFM head.

The motivation of this technological development is to build a tool capable of analyzing temperature distribution in modern nanodevices, nanostructures or nanocomposites (sub-40nm transistors, SETs, biochemical interfaces, graphene structures etc.). Moreover, the combination of the concepts of AFM cantilever and thermoresistive probe is a solution for mixed measurements e.g. thermal and electrical probing.

The device is built by microfabrication techniques [11, 10]. The cantilever is made with silicon (Si) body covered by a layer of silicon dioxide (SiO₂) that serves as an electrical insulator to the electrical conducting tracks which main body is in aluminum (Al) and which tip is in platinum (Pt),

a piezoresistive material. The conducting layer consists of four legs ending to the tip. The outer two legs are used to insert a controlled current and the inner two to measure the corresponding tip voltage drop yielding a four-wire resistance measurement method. For passive measurements the inserted current is set low to avoid significant heating while for active measurements the current tip heating is performed.

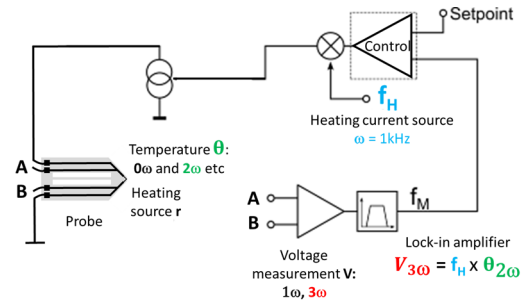


Fig. 1: Scheme of the control loop including a four point probe, a heating current source, a lock-in amplifier for voltage measurement and a regulator.

Figure 1 represent the setup used in the active mode working condition. In the active mode, the tip is heated by a modulated harmonic current source at a frequency ω , ranging from 1 to 10KHz, through the Joule effect and the thermoresistive tip temperature is evaluated thanks to voltage measurement yielding an evaluation of tip resistance change. For noise cancellation and for separation of harmonics, the voltage is passed through possibly several lock-in filter yielding voltage harmonics at $n\omega$ for various choices of n . The harmonic current should be regulated in order to keep a constant tip temperature during experiments with alternance of tip-sample contact and non-contact phases. A PID regulator is in use but yields insufficient performances. To overcome this limitation, we develop a model-based control law based on the Lyapunov method. The underlying model is the time-space two-scale electro-thermal model presented in [15] for the same SThM probe that allows for fast and precise computation of all modulated harmonic components near the tip as well as in the whole probe. To be efficient, the control law has also to account for an estimation of the heat source in the sample and for the delay in the lock-in filter based observation. Moreover, in this approach the experiment-based

model calibration is a prerequisite and will be discussed in detail.

The control approach has been derived in the framework of partial differential equations also referred as infinite dimensional systems, however here we present its finite dimensional counterpart i.e. expressed in matrix form. The infinite dimensional case will be published separately. The presented approach relies on a linearization around an operating point of the model, on the concept of Luenberger state observer, and the convergence relies to the Lyapunov method. For the observer, we combine the approaches of [1] to deal with delay in observations and of [3] and [22] to account for heat source identification.

The rest of the paper starts with a setup description in Section 2.. Section 3. presents our method of probe parameter calibration. The two-scale model is stated in Section 4., it serves as the model used for the control law detailed in Section 5..

2. Setup Description

The novel type of nano-sensor described in this paper, cf. Fig. 2 (a), is equipped with a sharp, conductive tip, cf. Fig. 2 (a) and (b), an integrated deflection sensor, and an actuation system. A modification of a double sided silicon micro-machining process developed for manufacturing of piezo-resistive AFM micro-probes has been adapted to fabricate SThM sensors [7].

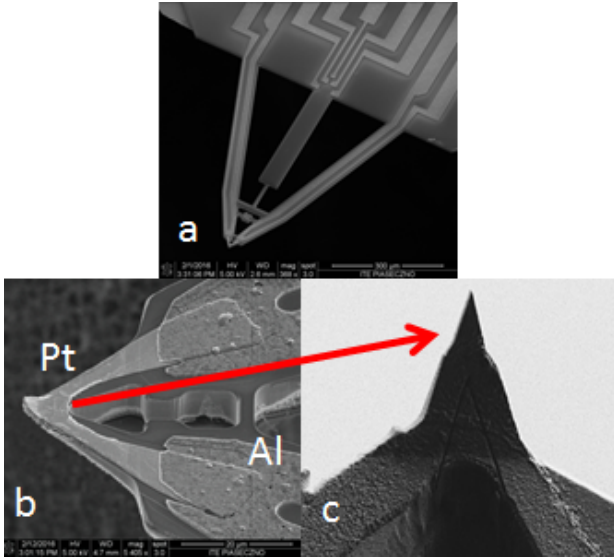


Fig. 2: New probe design (a) global view of the optimized design according to optimization rules in [21] (b) 3D tip before FIB milling (c) tip after FIB milling

The SThM/ECM probes on the market are based on bulky and complicated optical deflection sensors [13]. Therefore, their application in small SEM chambers is difficult. The proposed nano-probes are integrated with piezoresistive deflection detection, which will significantly improve the system versatility and will enable new applications also in narrow environments as vacuum chambers.

The new SThM nano-probes are designed to operate in two modes. They can be used as a passive thermo-sensing element or as an active heat flux meter. In the latter case, a larger AC current in the range of 1-10 kHz is passed

through the resistive tip probe leading to heat dissipation and a heat flow through the tip sample contact into the sample as shown in Fig. 1. The power that is required to maintain a constant temperature depends (among others) on the local thermal conductivity of the sample. During active measurements temperature of the tip is increased by 20-30 K above room temperature. According to the applications, developed SThM nanoprobe will enable surface contact measurements at load force ranging from 10 nN up to 1 μ N. The load force will be detected with the resolution of 10 pN in the bandwidth of 100 Hz. The low load forces as well as sub-nanometer vertical spatial resolution will be needed in investigations of graphene and molecular samples, whereas the high force will be applied in investigations of high-k insulators.

Going more in details, the body of the probe is made of silicon (Si) covered by an electric insulator layer in silicon dioxide (SiO₂), and then by a platinum (Pt) conductor layer. The latter consists of four legs ending to the tip. In active measurement mode, the two middle legs conduct a controlled heating current with the aim to keep the thermoresistive tip at a constant temperature. The two outer legs are for sensing the tip temperature. The heating current is harmonic at a frequency ω with amplitude modulation and the tip temperature is evaluated from lock-in amplifications which reference signals are multiples of ω . An extensive study of this SThM probe, taking into account the full electro-thermo-mechanical behavior in the static regime, has been carried out and reported in [21]. Detailed sensitivity analysis and optimization were investigated.

3. Parameter calibration

The physical parameters taken into account in the thermo-electrical effects considered in this paper are the electrical conductivity, the thermal conductivity, the temperature coefficient of resistance, the density and the specific heat denoted by σ^0 , k , TCR , ρ and c .

We distinguish between parameters well established from the bibliography of those to be calibrated. The material parameters of thin layers can deviate from known literature bulk values. In small dimensions the surface and edge effects cannot be neglected compared to the volume effects and additionally the structure of the layer will depend on the manufacturing processing parameters. We consider that the density and the specific heat are neither thickness nor process dependent, so we adopt their bulk values. In the opposite, the electrical conductivity, the thermal conductivity, the temperature coefficient of resistance are assumed to depend strongly on the fabrication process and of the layer thickness, so they must be determined in each particular case. For the sake of illustration of the layer thickness dependency of these parameters, the resistivity $1/\sigma^0$ of a 50 nm thick sputter deposited platinum is found to be equal to $3.0e-7 \Omega.m$ in [12] that may be compared to a resistivity of $1e-7 \Omega.m$ for bulk. Thanks to the Wiedemann-Franz law [4, 19], the thermal conductivity k can be deduced from the electrical conductivity through the formula $k/\sigma^0 = L \times T$ with T the absolute temperature and $L = 2.44e-8 \Omega/K^2$ the Lorentz number. But, for thin films, according to [5], the Wiedemann-Franz law relating the ratio k/σ^0 to temperature still holds but for a Lorentz number depending on the layer thickness and material. According to [20, 12], for

a 50 nm thin platinum layer fabricated by electron beam-physical vapor deposition $L = 5e-8 W.\Omega/K^2$ resulting in $k = 70.35 W/(m.K)$ at 300 K. From [12] the temperature coefficient of resistance (TCR) of platinum is $2.0e-3 K^{-1}$ for a 50 nm thin platinum layer compared to $3.9e-3 K^{-1}$ for bulk.

Calibration of physical parameters may be made according to several procedures. One approach is to measure the characteristics of materials with dedicated experiments. At each change of materials or manufacturing process or layer thicknesses these experiences need to be re-done. An alternative is to perform the calibration of a particular probe by combining experimental measurements on the probe with model simulation results. For this, we design a family of experiments which results contain sufficient information on the parameters and then the model parameters are adjusted to coincide with the experimental measurements using an optimization procedure.

Our results are obtained with the SIMBAD optimization and calibration tool developed in the FEMTO-ST institute linked with COMSOL through MATLAB. We take into account the thermal diffusion, the Joule heating and the thermo-resistance phenomena in three models corresponding to different operating modes: a static model for constant DC sources, a steady state harmonic model for sources with constant DC and harmonic components, and a transient model for sources which DC and modulated harmonic components.

The simulation is made sufficiently rapid thanks to a multi-scale model recalled in Section 4. that is valid for DC heating sources and sufficiently high heating frequencies, namely larger than few kHz. Besides its simulation speed, it has the advantage of accurately calculate the $v_{1\omega}$ and $v_{3\omega}$ components of the electrical potential used for the measurement. This model can be used for transient phenomena. A simplified version operates faster for stationary harmonic phenomena. The calibration work uses the multi-scale model simplified for stationary harmonic sources and solutions.

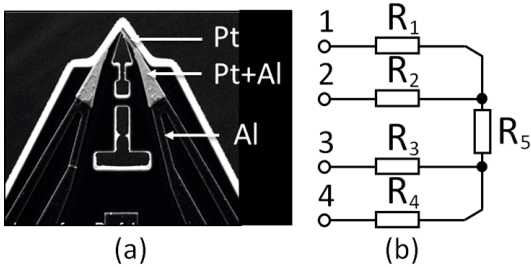


Fig. 3: (a) Top view of the probe with the conducting tracks made of Al, Pt+Al or Pt layers (b) simplified scheme of the probe as a four ports and five resistances circuit

Experiment #1 *three independent resistance measurements at ambient temperature:* with four ports, only three independent voltages can be directly measured, for instance 1-2, 1-3, 1-4 with the notations in Fig. 3 (b). For a sufficiently low current preventing heating, this provides the

	σ^0 S/m	k W/(m·K)	TCR 1/K	ρ kg/m ³	c J/(kg·K)
Al	X	X	X	Bib	Bib
Pt	X	X	X	Bib	Bib
Al+Pt	X	X	X	Bib	Bib
SiO2	⊥	Bib	⊥	Bib	Bib
Si100	⊥	Bib	⊥	Bib	Bib

Fig. 4: the parameters to be calibrated are marked with crosses, those known from bibliography are indicated with "Bib" and those not useful are with a "⊥"

values of the resistances of three branches at ambient temperature. We assume two symmetry relations $R_1 = R_4$ and $R_2 = R_3$, so the three resistances R_1 , R_2 and R_5 can be determined and then the values of R_3 and R_4 follow.

Experiment #2 *Three independent resistance measurements at a sequence of ambient temperatures with small DC or harmonic currents:* a temperature is imposed through the boundary conditions at the junction with the base. The three measurements provide the linear dependence $R_i(1 + TCR_i(T - T_0))$ of the resistances in the temperature where TCR_i stands for the *global* TCR of the i^{th} resistance. The source of current is a DC source or a harmonic source with frequency ω and the measured voltage is the DC voltage or the $\cos(\omega t)$ and $\sin(\omega t)$ -components of the voltage. The source is low to prevent tip heating.

Experiment #3 *Harmonic heating current and $v_{1\omega}$ and $v_{3\omega}$ measurements:* A harmonic current source is imposed to the ports 1 or 2 to heat the tip. The $\cos(\omega t)$, $\sin(\omega t)$, $\cos(3\omega t)$ and $\sin(3\omega t)$ components of the voltage are measured. All parameters of the tip are involved.

Here, we report a feasibility study carried out with numerical simulations only. Precisely, the experimental data are substituted by computed values using our models and arbitrary coefficients. The goal is to show which coefficient can be recovered before application to experimental results.

In each case, the study starts with a sensitivity analysis of the measurement about the unknown parameters. Then, the coefficients which are the most sensitive for a set of features are optimized to minimize the errors between experimental and model results for a part of the experimental results while the others are used to validate the optimal result. For the sake of computation time reduction, a metamodel is established from direct simulations before to be used in the optimization procedure. Our conclusion is that Experiment #1 yields a good calibration of the platinum and aluminum electrical conductivities and that of the Al+Pt composite layer is with negligible influence on the results. Once these conductivities are set, Experiment #2 provides a good calibration of the TCR of aluminum and platinum and is insensitive to that of the Al+Pt layer. Finally, when all the previously calibrated coefficients are set, Experiment #3 allows to calibrate the thermal coefficients of platinum and aluminum but not of the Al+Pt layer still appearing as lowly influential.

4. A time-space two-scale model

We state a slight variation of the time-space two-scale electrothermal model of the probe introduced in [15]. It constitutes a fundamental key in our approach of probe temperature control by modulated harmonic sources. After recalling the thermoelectric system and the space and time scales involved in the device behavior, the two-scale model is stated and new simulation results are provided and commented.

4.1 Governing equations

The heat diffusion in the probe and in the sample is governed by the heat equation $\rho c \partial_t \theta + \text{div } \mathbf{q} = r$ in the region Ω^{th} with unknown θ the difference between the absolute temperature and the ambient temperature. The coefficient r is for a radiative source and \mathbf{q} is the heat flux defined from the Fourier law $\mathbf{q} = -k \nabla \theta$. At the probe clamping part, the relative temperature θ is assumed to vanish and the tip-sample interaction is modeled by an interfacial resistance condition $\mathbf{q} \cdot \mathbf{n} = -G[\theta]$ between the normal flux and the temperature jump, where \mathbf{n} represents the outward unit normal to the boundary. The interface condition between layers is with a continuous temperature and heat flux. The other boundaries are assumed to be thermally insulated.

In absence of volume source of charges, the current density \mathbf{J} is governed by the conservation of charges $\text{div } \mathbf{J} = 0$ in a region $\Omega^{el} \subset \Omega^{th}$, and in a conductor or a semi-conductor it satisfies the Ohm law $\mathbf{E} = \boldsymbol{\rho}^{el} \mathbf{J}$ where $\mathbf{E} = (E_i)_{i=1,\dots,3} = -\nabla \varphi$ is the electric field, φ the electric potential and $\boldsymbol{\rho}^{el}$ the resistivity tensor. These equations are completed by imposing a controlled AC or DC current source in the heating branch $\int_{\Gamma_1^{el}} \mathbf{J} \cdot \mathbf{n} ds = j_d$. Moreover, a zero current source is imposed in the measurement branch and all the other boundaries are electrically insulated. The AC heating current is at a frequency ω and is modulated in amplitude. The volume heat source generated by a current density in a conductor or a semi-conductor is given by the Joule's law $r = \mathbf{E} \cdot \mathbf{J} = \boldsymbol{\rho}^{el}(\theta) |\mathbf{J}|^2$. The electrical resistivity of most materials changes with temperature. If the temperature does not vary too much, a linear approximation is typically used $\boldsymbol{\rho}^{el}(\theta) = \boldsymbol{\rho}_0^{el}(1 + \alpha \theta)$ where α is the temperature coefficient of resistivity (TCR) of materials, and $\boldsymbol{\rho}_0^{el}$ the resistivity at ambient temperature. The lock-in filter measurements are designed at various possible frequencies $n\omega$ for $n = 0, 1, 2, 3, \dots$ yielding the measurements $v_n^c = \frac{1}{\Delta t} \int_{t-\Delta t}^t \varphi(\sigma) \cos(n\omega\sigma) d\sigma$ and $v_n^s = \frac{1}{\Delta t} \int_{t-\Delta t}^t \varphi(\sigma) \sin(n\omega\sigma) d\sigma$ integrating over an integer number of periods. For instance the classical 3ω -measurement method [2] consists in measuring v_3^c and v_3^s . It generates a delay in observation, so in view of fast operations, the frequency ω should be chosen relatively high, but not too much since the amplitude of the 3ω -component decreases when the frequency increases.

4.2 Time and space scales

In a heat diffusion process, the time and space scales are related as $\rho c / T = k^{th} / L^2$ where T and L are the characteristic time and length scales. The work [15] shows that this system has two time scales T_M and T_m , namely the time scales of the DC component and of the harmonic components that we also refer as the macro- and micro-

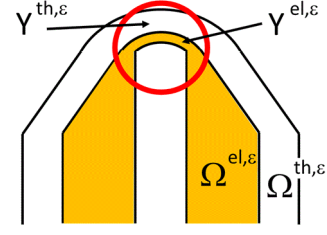


Fig. 5: The domain $Y^\varepsilon = Y^{th,\varepsilon} \cup Y^{el,\varepsilon}$ where the high frequency temperature is localized and $\Omega^\varepsilon = \Omega^{th,\varepsilon} \cup \Omega^{el,\varepsilon}$ the complementary part. The electric conductor is in yellow.

time-scales as usual in multi-scale modeling methods. The DC-temperature field is spread out in the full probe when the AC-temperature field is concentrated near the heating part. So, two space scales L_M and L_m correspond to the two time scales and both these time and space scales are the foundation of the asymptotic model stated in this section. We denote by $\varepsilon_t = \frac{T_m}{T_M}$ and $\varepsilon_x = \frac{L_m}{L_M}$ the corresponding time and space scale ratios, they satisfy the relation $\varepsilon_t = \varepsilon_x^2$, and ε_t is considered as the single small parameter of this problem. The macroscopic length scale L_M is equal to the probe length and the microscopic time scale is $T_m = 2\pi/\omega$. The two other scales follow: $L_m = \sqrt{\frac{T_m k^{th}}{\rho c}}$ and $T_M = \frac{\rho c L_M^2}{k^{th}}$. In total, the small parameter of the asymptotic problem is $\varepsilon_t = 2\pi/(L_M^2 \omega)$.

4.3 The two-scale model

For simplicity, we use the notation ε instead of ε_t . The time interval $[0, T]$ is split into subintervals (t_i, t_{i+1}) where $t_i = i \times \varepsilon$ for $i = 0, \dots, T/\varepsilon - 1$ and the operator \mathcal{T} of two-scale transform maps any function $f(t)$ into the function $\mathcal{T}(f)(t, \tau) = f(t_i + \varepsilon\tau)$ for any $t \in (t_i, t_{i+1})$ and $\tau \in (0, 1)$ that is actually defined over $(t, \tau) \in (0, T) \times (0, 1)$ and so is called a time-two-scale function. Applying this transformation to a modulated ε -periodic signal captures both the modulation and the periodic signal with the two scales. Applying this idea to the thermal and electrical fields, we obtain the equations of their two-scale transforms in the high-frequency limit, i.e. when ε vanishes. The solutions of this limit model, after being restated in the physical time, produces an approximation for "high" but not infinite frequencies. In the probe the heater is very small, so we consider its size in the range of ε_x and are led to consider a neighbourhood $Y^{th,\varepsilon}$ of the heating source and its complementary $\Omega^{th,\varepsilon}$. A similar distinction is made between $Y^{el,\varepsilon}$ and $\Omega^{el,\varepsilon}$ for the electric conductor, see Fig. 5. For simplicity, the center of $Y^{th,\varepsilon}$ is set as the origin of the coordinates so $Y^{th,\varepsilon} \subset \{x \in \mathbb{R}^3 \mid |x| \leq \lambda\sqrt{\varepsilon}\}$ for a given λ . Finally, for the sake of coherency the assumption of thin heating part led us to assume that the conducting layer is also scalable by $\sqrt{\varepsilon}$. The time-space multi-scale model results from putting these assumptions all together and finding the asymptotic behaviour of the model when ε vanishes. It is made with four equations expressed in the domains $\Omega^{th,0}$, $\Omega^{el,0}$, $Y^{th,0} = Y^{th,\varepsilon}/\varepsilon_x$ and $Y^{el,0} = Y^{el,\varepsilon}/\varepsilon_x$, with the fields $\varphi^{0,\Omega}$, $\theta^{0,\Omega}$, $\varphi^{1,Y}$ and $\theta^{1,Y}$ defined in $\Omega^{el,0}$, $\Omega^{th,0}$, $Y^{el,0}$, $Y^{th,0}$ respectively, and with the coefficients $m^0 = \frac{\rho c}{\rho^{si} c^{si}}$, $k^0 = \frac{T_M k}{\rho^{si} c^{si} L_M^2}$, $r^0 = \frac{T_M r}{\rho^{si} c^{si}}$, $G^0 = \frac{\varepsilon_x T_M G}{\rho^{si} c^{si} L_M}$,

$b^0 = \frac{V_0^2 T_M}{\rho_{Si} c_{Si} L_M^2 \rho_0^{el}}$, $\kappa^0 = \frac{\rho_0^{el, Pt}}{\rho_0^{el}}$, $j_d^0 = \frac{L_M \rho_0^{el, Pt} j_d}{\sqrt{\varepsilon_x} V^0}$ and $\omega^0 = \omega \varepsilon$ with V^0 a scaling of the electrical potential. The electrical potential $\varphi^{0, \Omega}$ is constant in the thickness of the layer and is solution to

$$-\overline{\text{div}}\left(\frac{\kappa^0}{1 + \alpha\theta^{0, \Omega}} \nabla \varphi^{0, \Omega}\right) = 0 \quad (1)$$

in $\Omega^{el, 0}$, with the controlled current source $\int_{\Gamma_{cur, 0}} \frac{\kappa^0}{1 + \alpha\theta^{0, \Omega}} \nabla \varphi^{0, \Omega} \cdot \bar{n} ds(x) = j_d^0$ the two-scale transform of j_d , and the same other homogeneous boundary conditions as φ . The temperature field $\theta^{0, \Omega}$ is independent of τ , so it corresponds to the DC-component solution of the heat equation

$$\begin{cases} m^0 \frac{\partial \theta^{0, \Omega}}{\partial t} - \text{div}(k^0 \nabla \theta^{0, \Omega}) \\ = \frac{\int_0^1 b^0 |\nabla \varphi^{0, \Omega}|^2 + r^0 d\tau}{1 + \alpha\theta^{0, \Omega}} \end{cases} \quad (2)$$

in $\Omega^{th, 0}$ which source term is the effective heating, i.e. its average in the fast time variable. It satisfies the same interface condition as θ and is continuous through the tip-sample interface. The latter is an artefact of the asymptotic approach, that might be corrected with a higher order term for a better precision. The field $\theta^{1, Y}$ is solution of a heat equation at the small scale with a source term including only harmonic components,

$$\begin{aligned} m^0 \frac{\partial \theta^{1, Y}}{\partial \tau} - \text{div}_y(k^0 \nabla_y \theta^{1, Y}) \\ = \frac{b^0 |\nabla \varphi^{0, Y}|^2 + r^0 - \int_0^1 b^0 |\nabla \varphi^{0, Y}|^2 + r^0 d\tau}{1 + \alpha\theta^{0, Y}} \end{aligned} \quad (3)$$

in $Y^{th, 0}$. It satisfies the transmission conditions $k^0 \nabla_y \theta^{1, Y} \cdot \mathbf{n}_y = G^0[\theta^{1, Y}]$ at the tip-sample interface together with the continuity of the heat flux, and the thermal insulation boundary condition at the other boundaries, except at the boundary created by the localization procedure where a vanishing temperature condition holds. Finally, the equation of $\varphi^{1, Y}$ of the electrical potential is fed by oscillations produced by the product of those in $\varphi^{0, Y}$ and $\theta^{1, Y}$,

$$\begin{aligned} -\text{div}_y\left(\kappa_0^0 \frac{\nabla_y \varphi^{1, Y}}{1 + \alpha\theta^{0, Y}}\right) \\ = -\alpha \text{div}_y\left(\kappa_0^0 \frac{\theta^{1, Y} \nabla_y \varphi^{0, Y}}{(1 + \alpha\theta^{0, Y})^2}\right) \end{aligned} \quad (4)$$

in $Y^{el, 0}$, when its other boundary conditions are of the same kind as those of $\varphi^{0, Y}$ but homogeneous. Then, the approximation in the physical time-space of the temperature and the electric potential fields are obtained by inverse scalings $\theta \approx \theta^{0, \Omega}(t, t/\varepsilon, x) + \varepsilon \theta^{1, Y}(t, t/\varepsilon, x/\sqrt{\varepsilon})$ and $\varphi \approx \varphi^{0, \Omega}(t, t/\varepsilon, \bar{x}, x_3/\sqrt{\varepsilon}) + \varepsilon \varphi^{1, Y}(t, t/\varepsilon, x/\sqrt{\varepsilon})$. The lock-in filter measurements of the voltage on a time interval Δt , multiple of ε , is restated as a discrete measurement using the two-scale transform,

$$v(t) \approx \frac{1}{\Delta t} \int_{t-\Delta t}^t \int_0^1 (\varphi^{0, \Omega} + \varepsilon \varphi^{1, Y})(s, \tau) w(\tau) d\tau ds$$

where $w(\tau)$ holds for $\phi_c^n(\tau) = \cos(n\omega^0 \tau)$ or $\phi_s^n(\tau) = \sin(n\omega^0 \tau)$.

4.4 Simulation results

Our implementation is in the case of a small temperature, so that $(1 + \alpha\theta^0) \approx 1 - \alpha\theta^0$, and we keep only the first significant terms of the Fourier series $\theta^0(t, x) \approx c_0(t, x)$, $\theta^1(t, \tau, x/\sqrt{\varepsilon}) = c_2(t, x)\phi_c^2(\tau) + s_2(t, x)\phi_s^2(\tau)$, $\varphi^0(t, x) \approx a_1(t, x)\phi_c^1(\tau) + b_1(t, x)\phi_s^1(\tau)$ and $\varphi^1(t, \tau, x) \approx a_3(t, x)\phi_c^3(\tau) + b_3(t, x)\phi_s^3(\tau)$, so that only the related functions c_n , s_n , a_n and b_n need to be computed. Thus, the computation time is independent of the current source frequency.

The two-scale model simulations have been compared with a direct simulation in [15]. For a 1kHz frequency source, the ratio between their computation time is in the range of 15 – 20 and increases with the frequency. The error between the two simulation results is generally in the range of few percents on the DC-temperature θ^0 and the harmonic part θ^1 if the accuracy of the direct simulation is sufficient. It is worthwhile to mention that in the direct simulation we did not yet obtained a visible electrical field φ^1 preventing the simulation of the 3ω -measurement method.

Two-scale model simulation results for the higher frequency current source, namely $\omega = 10$ kHz are reported in Fig. 6, 7, 8 and 9. The current sources j_d are combinations a DC-source $j_{dc} = 4$ mA, of an AC-source $j_{ac} = 4$ mA $\times \sin(\omega t)$ and of a smoothed Heaviside step function $H_\sigma(t - t^*)$ centered at $t^* = 10^{-3}$ s and with smoothing parameter $\sigma = 10^{-4}$ for a sharp step and $\sigma = 10^{-3}$ for a smooth step. Precisely, the source $j_d = (1 + H_\sigma(t - t^*)) \times j_{dc} + j_{ac}$ is referred as with DC source variations and $j_d = j_{dc} + (1 + H_\sigma(t - t^*)) \times j_{ac}$ as with AC source variation. The smoothing parameter σ is the time duration of the transition. In all figures, the blue curve corresponds to a smooth source variation, and the red curve to a sharp source variation.

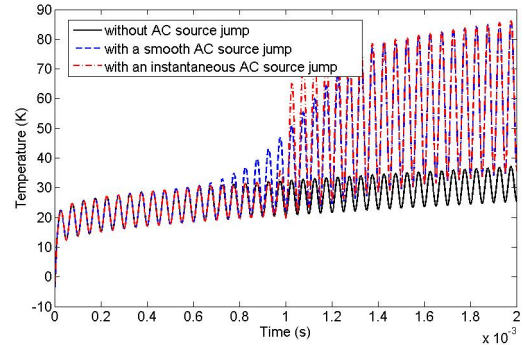


Fig. 6: Response of the tip temperature to a mixed AC-DC current source with abrupt or smooth variations in AC source variations

The expected effects are well recovered. Indeed, Fig. 6 and 7 show that the AC-source contributes to the temperature oscillation amplitude and the DC-source contributes to the average value of the temperature. The response of the temperature to the source variation is instantaneous.

Fig. 8 and 9 show that the 3ω -voltage is only sensitive to the AC-source variations. This is a trivial phenomena

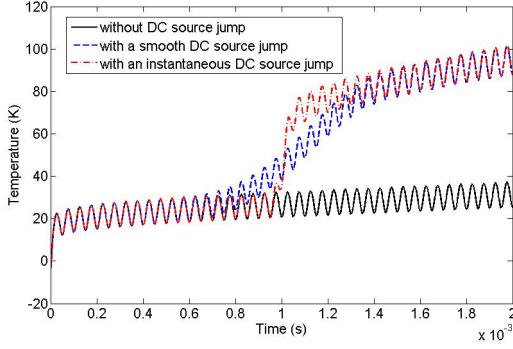


Fig. 7: Response of the tip temperature to a mixed AC-DC current source with abrupt or smooth variations in DC source variations

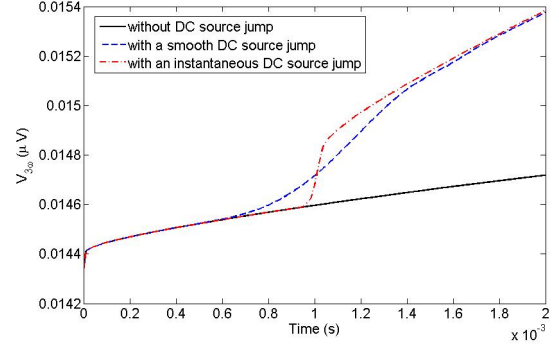


Fig. 9: Response of the amplitude of the 3ω -voltage component at the tip to a mixed AC-DC current source with abrupt or smooth variations of DC source

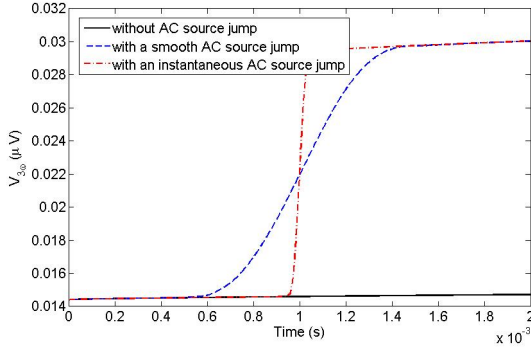


Fig. 8: Response of the amplitude of the 3ω -voltage component at the tip to a mixed AC-DC current source with abrupt or smooth variations of AC source

since the 3ω -voltage is a product of the tip electric resistance and the AC-source.

5. Regulation of the tip temperature

We consider a probe tip heated by a modulated harmonic current source such that its scaled two-scale transform $j_d^0(t, \tau) \approx u(t) \cos(\omega^0 \tau)$ where the modulation u is the control to be determined so that the time-quadratic mean of the tip temperature reaches an objective value T^* . The case $\omega = 0$ corresponding to a DC current source is covered by our approach. The heat source is assumed to be unknown, but depending on an unmodulated harmonic source, so its two-scale transform has the form $r^0(t, \tau) \approx s \times \cos(\ell \omega t / \varepsilon)$ for a positive integer ℓ and with an unknown constant s to be estimated during the regulation phase. We start by presenting a general method for reconstructing the state of the system. Then, it is shown in Sections 5.2 and 5.3 how it may be applied for tip temperature control when the source is DC or harmonic.

5.1 A Luenberger observer

As detailed in Sections 5.2 and 5.3, for each kind of heating current corresponds a particular part of the two-scale model to be used. After decomposition over a family of harmonics and discretization by a Finite Element Method, it has the form of a nonlinear algebro-differential

equation,

$$\begin{cases} \frac{d\mathbf{x}_1}{dt} = \mathbf{F}_1(\mathbf{x}_1, \mathbf{x}_2, s) \\ \text{and } \mathbf{0} = \mathbf{F}_2(\mathbf{x}_1, \mathbf{x}_2, u) \text{ for } t > 0, \\ \mathbf{v} = \int_{t-\Delta t}^t \mathbf{C}\mathbf{x}_2(\sigma) d\sigma \text{ for } t \geq \Delta t, \end{cases} \quad (5)$$

with the initial condition $\mathbf{x}_1 = \mathbf{z}$ at $t = 0$, where $\mathbf{x} = (\mathbf{x}_1, \mathbf{x}_2)$, s , u , v , \mathbf{z} stand for the state, the unknown heat source, the control modulation, the observation and the initial state. Then, for constant reference sources s^0 and u^0 , we define $\mathbf{x}^0 = (\mathbf{x}_1^0, \mathbf{x}_2^0)$ as the solution to the stationary equation, and a perturbation $(\bar{\mathbf{x}}_1, \bar{\mathbf{x}}_2) \approx (\mathbf{x}_1 - \mathbf{x}_1^0, \mathbf{x}_2 - \mathbf{x}_2^0)$ solution to the linearized system about $(\mathbf{x}_1^0, \mathbf{x}_2^0)$,

$$\begin{cases} \frac{d\bar{\mathbf{x}}_1}{dt} = \mathbf{A}_{11}\bar{\mathbf{x}}_1 + \mathbf{A}_{12}\bar{\mathbf{x}}_2 + \mathbf{D}\bar{s}, \\ \mathbf{0} = \mathbf{A}_{21}\bar{\mathbf{x}}_1 + \mathbf{A}_{22}\bar{\mathbf{x}}_2 + \mathbf{B}\bar{u} \text{ for } t > 0, \\ \bar{\mathbf{v}} = \int_{t-\Delta t}^t \mathbf{C}\bar{\mathbf{x}}_2(\sigma, \tau) d\sigma \text{ for } t \geq \Delta t, \end{cases} \quad (6)$$

with the sources $\bar{s} = s - s^0$, $\bar{u} = u - u^0$ and the initial condition $\bar{\mathbf{x}}_1 = \bar{\mathbf{z}} = \mathbf{z} - \mathbf{x}_1^0$. In the following, \mathbf{A}_{22} is always assumed to be invertible. Since it is known that for an arbitrary small $\eta > 0$, $\bar{\mathbf{v}} = \bar{\xi}(t, 0) + O(\eta)$ where $\bar{\xi}(t, z)$ is the solution of $\frac{\partial \bar{\xi}}{\partial t} - \eta \frac{\partial^2 \bar{\xi}}{\partial z^2} - \frac{\partial \bar{\xi}}{\partial z} = \mathbf{C}\bar{\mathbf{x}}_2$ for $t > 0$ and $z \in (0, \Delta t)$ with boundary conditions $\eta \frac{\partial \bar{\xi}}{\partial z}(t, 0) = 0$, $\bar{\xi}(t, \Delta t) = 0$ and homogeneous initial condition, we introduce a Luenberger observer $(\hat{\mathbf{x}}_1, \hat{\mathbf{x}}_2, \hat{s}, \hat{\xi})$ of $(\bar{\mathbf{x}}_1, \bar{\mathbf{x}}_2, \bar{s})$ solution for $t > 0$ of

$$\begin{cases} \frac{d\hat{\mathbf{x}}_1}{dt} = \mathbf{A}_{11}\hat{\mathbf{x}}_1 + \mathbf{A}_{12}\hat{\mathbf{x}}_2 + \hat{\mathbf{g}} \\ \mathbf{0} = \mathbf{A}_{21}\hat{\mathbf{x}}_1 + \mathbf{A}_{22}\hat{\mathbf{x}}_2 + \mathbf{B}\hat{u}, \\ \frac{d\hat{s}}{dt} = -\lambda \gamma_1^T \Xi_{z=0}^T \hat{\mathbf{v}}, \\ \frac{\partial \hat{\xi}}{\partial t} - \eta \frac{\partial^2 \hat{\xi}}{\partial z^2} - \frac{\partial \hat{\xi}}{\partial z} = \mathbf{C}\hat{\mathbf{x}}_2 + \Xi_z \hat{\mathbf{g}}, \\ \eta \frac{\partial \hat{\xi}}{\partial z}(t, 0) = 0, \hat{\xi}(t, \Delta t) = 0 \\ \text{and } \hat{\mathbf{v}} = \hat{\xi}(t, 0), \end{cases} \quad (7)$$

with homogeneous initial conditions in $\widehat{\mathbf{x}}_1$, \widehat{s} and $\widehat{\xi}$. Here, $\widehat{\mathbf{g}} = \mathbf{D}\widehat{s} + \Xi_{z=0}^T(\widehat{v} - \bar{v}) + \gamma_1 \frac{d\widehat{s}}{dt}$, $\Xi_z = -\mathbf{F}\Lambda_z$, $\mathbf{F} = \mathbf{C}\mathbf{A}_{22}^{-1}\mathbf{A}_{21}$, Λ_z is solution to the boundary value problem

$$-\eta \frac{\partial^2 \Lambda_z}{\partial z^2} - \frac{\partial \Lambda_z}{\partial z} + \mathbf{E}\Lambda_z = -\mathbf{I} \quad (8)$$

for $z \in (0, \Delta t)$ with the boundary conditions $\Lambda_{z=\Delta t} = \eta \frac{\partial \Lambda_{z=0}}{\partial z} = 0$, the matrix $\mathbf{E} = \mathbf{A}_{11} - \mathbf{A}_{12}\mathbf{A}_{22}^{-1}\mathbf{A}_{21}$ and $\gamma = (\gamma_1, \gamma_2)$ the solution to

$$\begin{cases} \mathbf{0} = \mathbf{A}_{11}\gamma_1 + \mathbf{A}_{12}\gamma_2 + \Xi_{z=0}^T \Xi_{z=0} \gamma_1 + \mathbf{D}, \\ \mathbf{0} = \mathbf{A}_{21}\gamma_1 + \mathbf{A}_{22}\gamma_2. \end{cases}$$

If the matrix $\mathbf{E} + \Xi_{z=0}^T \Xi_{z=0}$ is stable, then for any control \bar{u} the Luenberger observer is convergent in the sense that the difference between the estimation $\widehat{\mathbf{x}}$ and $\bar{\mathbf{x}}$ vanishes when t goes to infinity.

Remark 1 A similar approach is applicable when the first differential equation of the nonlinear system (5) is replaced by the algebraic equation $\mathbf{0} = \mathbf{F}_1(\mathbf{x}_1, \mathbf{x}_2, s)$. The first equation of the linearized system is replaced by $\mathbf{0} = \mathbf{A}_{11}\bar{\mathbf{x}}_1 + \mathbf{A}_{12}\bar{\mathbf{x}}_2 + \mathbf{D}\bar{s}$ and the Luenberger observer $\widehat{s}(t)$ of \bar{s} is solution of the system

$$\begin{cases} \frac{d\widehat{s}}{dt} = -\lambda \Xi(0)(\widehat{v} - \bar{v}), \\ \frac{\partial \widehat{\xi}}{\partial t} - \eta \frac{\partial^2 \widehat{\xi}}{\partial z^2} - \frac{\partial \widehat{\xi}}{\partial z} = \mathbf{C}\widehat{\mathbf{x}}_2 - \lambda \Xi(z)\Xi(0)(\widehat{v} - \bar{v}), \end{cases}$$

for $t > 0$ and $z \in (0, \Delta t)$, where $\widehat{v}(t) = \widehat{\xi}(t, 0)$, $\widehat{\xi}$ satisfies the same initial and boundary conditions as above, and $\Xi(z) = \mathbf{C}\mathbf{p}_2(\Delta t - z) + O(\eta)$ where $(\mathbf{p}_1, \mathbf{p}_2)$ is solution of the system $\mathbf{A}_{11}\mathbf{p}_1 + \mathbf{A}_{12}\mathbf{p}_2 + \mathbf{D} = \mathbf{0}$ and $\mathbf{A}_{21}\mathbf{p}_1 + \mathbf{A}_{22}\mathbf{p}_2 = \mathbf{0}$.

5.2 Measurement of a DC temperature

In case of a DC heat source s in a sample and choosing a DC control current, the lock-in measurement is done at $\omega = 0$ meaning doing an average over a time length Δt . Therefore, only the DC component θ^0 of the temperature is useful together with the electrical potential φ^0 which is a DC voltage in this case. For simplicity, we remove the superscript 0, so for instance the voltage measurement is $v = \int_{t-\Delta t}^t \varphi(\sigma) d\sigma$. For a reference steady state (θ_0, φ_0) corresponding to a heat source s_0 and a constant control u_0 , we introduce a perturbation $(\bar{\theta}, \bar{\varphi})$ solution to the linearized problem about (θ_0, φ_0)

$$\begin{cases} \rho C \partial_t \bar{\theta} = A_\theta \bar{\theta} + D_\theta \bar{\varphi} + \bar{s} \text{ in } \Omega^{th}, \\ A_\varphi \bar{\varphi} + D_\varphi \bar{\theta} = 0 \text{ in } \Omega^{el}, \end{cases}$$

with a current source \bar{u} and the heat source $\bar{s} = s - s_0$, where for shortness the precise expression of the linear operators A_θ , D_θ , A_φ and D_φ are not detailed here. The discretization of $\bar{\theta}$ and $\bar{\varphi}$ being denoted by $\bar{\mathbf{x}}_1$ and $\bar{\mathbf{x}}_2$, the discretized system has the structure of (6) allowing the use of the Luenberger observer. Finally, we choose the control

$$u = u^0 + \bar{u}^0 + \frac{1}{\beta} (\widehat{\mathbf{x}}_1 - \bar{\mathbf{x}}_1^0)^T \mathbf{A}_{12} \mathbf{A}_{22}^{-1} \mathbf{B}$$

where $(\bar{\mathbf{x}}_1^0, \bar{\mathbf{x}}_2^0, \bar{u}^0)$ is the solution of

$$\begin{cases} \mathbf{0} = \mathbf{A}_{11}\bar{\mathbf{x}}_1^0 + \mathbf{A}_{12}\bar{\mathbf{x}}_2^0 + \mathbf{D}\widehat{s}, \\ \mathbf{0} = \mathbf{A}_{22}\bar{\mathbf{x}}_2^0 + \mathbf{B}\bar{u}^0, \\ \mathbf{P}(\bar{\mathbf{x}}_1^0 + \mathbf{x}_1^0) = T^*, \end{cases}$$

where the third equation is the discretization of the temperature objective to be reached.

5.3 Measurement of an harmonic temperature

In case of an harmonic heat source $s \cos(2\omega^0 \tau)$, a modulated harmonic control $u(t) \cos(\omega^0 \tau)$ and a 3ω -lock-in measurement, we use Equations (1,3,4) of the two-scale model. Since the temperature θ^0 is independent of the fast time variable τ and α is in the range of 10^{-3} or less, for moderate temperature and a moderate precision requirement, we use the approximation

$$1 + \alpha \theta^0 \approx 1$$

without significant lost precision and get,

$$\begin{cases} -\overline{\text{div}}(\kappa^0 \overline{\nabla} \varphi^0) = 0 \text{ in } \Omega^{el,0} \\ m^0 \frac{\partial \theta^1}{\partial \tau} - \text{div}_y(k^0 \nabla_y \theta^1) = \\ b^0 (|\nabla \varphi^0|^2 - \int_0^1 |\nabla \varphi^0|^2 d\tau) \\ + s \cos(2\omega^0 \tau) \text{ in } Y^{th,0} \\ -\text{div}_y(\kappa^0 \nabla_y \varphi^1) = \\ -\alpha \text{div}_y(\kappa^0 \theta^1 \nabla_y \varphi^0) \text{ in } Y^{el,0} \end{cases} \quad (9)$$

with the control $u \cos(\omega^0 \tau)$ feeding φ^0 . The 3ω -observation reads,

$$v(t) = \frac{1}{\Delta t} \int_{t-\Delta t}^t \int_0^1 \varepsilon \varphi^1(\sigma, \tau) \cos(3\omega^0 \tau) d\tau d\sigma. \quad (10)$$

Two approaches are presented, one is doing a direct computation of s from an observation v . It generates an instantaneous discontinuous regulation. The other is a smoother control involving the Luenberger observer of s .

A direct approach For a given source modulation s , we state the control u so that a quadratic mean of the temperature θ^1 reaches an objective $T_{2\omega}^*$ to the tip: $\int_0^1 |\theta_{tip}^1|^2 d\tau = (T_{2\omega}^*)^2$. We use the decomposition $\varphi^0 = \Phi^0 \times u$ where Φ^0 is solution to $-\overline{\text{div}}(\kappa^0 \overline{\nabla} \Phi^0) = 0$ in $\Omega^{el,0}$ with current source $\cos(\omega^0 \tau)$. Thus $\theta^1 = \Theta_u^1 \times u^2 + \Theta_s^1 \times s$ where $m^0 \frac{\partial \Theta_u^1}{\partial \tau} - \text{div}_y(k^0 \nabla_y \Theta_u^1) = b^0 (|\nabla \Phi^0|^2 - \int_0^1 |\nabla \Phi^0|^2 d\tau)$ and $m^0 \frac{\partial \Theta_s^1}{\partial \tau} - \text{div}_y(k^0 \nabla_y \Theta_s^1) = \cos(2\omega^0 \tau)$. The objective equation reads

$$\int_0^1 |\theta_{tip}^1|^2 d\tau = \int_0^1 |\Theta_u^1 \times u^2 + \Theta_s^1 \times s|^2 d\tau = (T_{2\omega}^*)^2,$$

so u is solution to $a \times u^4 + 2b \times u^2 + c = 0$ with $a = \int_0^1 |\Theta_u^1|_{tip}^2 d\tau$, $b(s) = \int_0^1 |\Theta_u^1|_{tip} \Theta_s^1|_{tip}|^2 d\tau \times s$ and $c(s) = \int_0^1 |\Theta_s^1|_{tip}^2 d\tau \times s^2 - (T_{2\omega}^*)^2$. Finally, we keep only the solution

$$u = \left(\frac{-b(s) + \sqrt{b^2(s) - ac(s)}}{a} \right)^{1/2} \quad (11)$$

under the condition that the objective $T_{2\omega}^*$ is sufficiently large compared to s so that $c(s) < 0$.

An observer approach We decompose the control and the sample temperature amplitudes as $u = u_0 + \bar{u}$ and $s = s_0 + \bar{s}$ where \bar{u} and \bar{s} are small perturbations and introduce the state perturbation $(\bar{\varphi}^0, \bar{\theta}^1, \bar{\varphi}^1) \approx (\varphi^0 - \varphi_0^0, \theta^1 - \theta_0^1, \varphi^1 - \varphi_0^1)$, about a reference solution $(\varphi_0^0, \theta_0^1, \varphi_0^1)$ of the nonlinear problem (9). After linearization of the equation, decomposition of $\bar{\varphi}^0$, $\bar{\theta}^1$ and $\bar{\varphi}^1$ over the $1\omega^0$, $2\omega^0$ and $3\omega^0$ components respectively, and discretization thanks to a FEM, it results a linear system on the form (6) where \bar{x}_1 and \bar{x}_2 are the discretization of $\bar{\theta}^1$ and $(\bar{\varphi}^0, \bar{\varphi}^1)$. Thus Remark 1 applies and the control expression (11) is used where s is replaced by $s_0 + \hat{s}$ and u by $u_0 + \bar{u}$ which allows the determination of \bar{u} .

References

1. Nikolaos Bekiaris-Liberis and Miroslav Krstic. Lyapunov stability of linear predictor feedback for distributed input delays. *Automatic Control, IEEE Transactions on*, 56(3):655–660, 2011.
2. D. G. Cahill and R. O. Pohl. Thermal conductivity of amorphous solids above the plateau. *Physical review B*, 35(8):4067, 1987.
3. Jonathan Chauvin. Observer design for a class of wave equation driven by an unknown periodic input. In *Control Applications (CCA), 2012 IEEE International Conference on*, pages 922–926. IEEE, 2012.
4. GV Chester and A Thellung. The law of wiedemann and franz. *Proceedings of the Physical Society*, 77(5):1005, 1961.
5. Sun Rock Choi, Dongsik Kim, and Sung-Hoon Choa. Thermal diffusivity of metallic thin films: Au, sn, mo, and al/ti alloy. *International journal of thermophysics*, 27(5):1551–1563, 2006.
6. R.B. Dinwiddie, R.J. Pylkki, and P.E. West. Thermal conductivity contrast imaging with a scanning thermal microscope. *Thermal conductivity*, 22:668–668, 1993.
7. K Domanski, P Janus, P Grabiec, R Perez, N Chaillet, S Fahlbusch, A Sill, and S Fatikow. Design, fabrication and characterization of force sensors for nanorobot. *Microelectronic engineering*, 78:171–177, 2005.
8. T Gotszalk, P Grabiec, and Ivo W Rangelow. Calibration and examination of piezoresistive wheatstone bridge cantilevers for scanning probe microscopy. *Ultramicroscopy*, 97(1):385–389, 2003.
9. T Ivanov, T Gotszalk, P Grabiec, E Tomerov, and IW Rangelow. Thermally driven micromechanical beam with piezoresistive deflection readout. *Microelectronic engineering*, 67:550–556, 2003.
10. P. Janus, D. Szmigielski, M. Weisheit, G. Wielgoszewski, Y. Ritz, P. Grabiec, M. Hecker, T. Gotszalk, P. Sulecki, and E. Zschech. Novel sthm nanoprobe for thermal properties investigation of micro-and nanoelectronic devices. *Microelectronic Engineering*, 87(5):1370–1374, 2010.
11. Paweł Janus, Piotr Grabiec, Andrzej Sierakowski, Teodor Gotszalk, Maciej Rudek, Daniel Kopiec, Wojciech Majstrzyk, Guillaume Boetsch, and Bernd Koehler. Design, technology, and application of integrated piezoresistive scanning thermal microscopy (sthm) microcantilever. In *SPIE Scanning Microscopies*, pages 92360R–92360R. International Society for Optics and Photonics, 2014.
12. S. Jónsson. Nonlinear thermal electric analysis of platinum microheaters. 2009.
13. William P King, Bikramjit Bhatia, Jonathan R Felts, Hoe Joon Kim, Beomjin Kwon, Byeonghee Lee, Suhas Somnath, and Matthew Rosenberger. Heated atomic force microscope cantilevers and their applications. *Annual Review of Heat Transfer*, 16(16), 2013.
14. William P King, Thomas W Kenny, Kenneth E Goodson, Graham LW Cross, Michel Despont, Urs T Dürig, Hugo Rothuizen, Gerd Binnig, and Peter Vettiger. Design of atomic force microscope cantilevers for combined thermomechanical writing and thermal reading in array operation. *Microelectromechanical Systems, Journal of*, 11(6):765–774, 2002.
15. M Lenczner, B Yang, M Abaidi, A Bontempi, D Teyssieux, B Koehler, and P Janus. Modeling and model-based control of temperature in an sthm probe. In *Thermal, Mechanical and Multi-Physics Simulation and Experiments in Microelectronics and Microsystems (EuroSimE), 2015 16th International Conference on*, pages 1–7. IEEE, 2015.
16. A. Majumdar, J.P. Carrejo, and J. Lai. Thermal imaging using the atomic force microscope. *Applied Physics Letters*, 62(20):2501–2503, 1993.
17. Russell J Pylkki, Patrick J Moyer, and Paul E West. Scanning near-field optical microscopy and scanning thermal microscopy. *Japanese journal of applied physics*, 33(6S):3785, 1994.
18. IW Rangelow, T Gotszalk, P Grabiec, K Edinger, and N Abedinov. Thermal nano-probe. *Microelectronic engineering*, 57:737–748, 2001.
19. F Völklein, H Reith, TW Cornelius, M Rauber, and R Neumann. The experimental investigation of thermal conductivity and the wiedemann–franz law for single metallic nanowires. *Nanotechnology*, 20(32):325706, 2009.
20. Zhang Xing, Zhang Qing-Guang, Cao Bing-Yang, Fujii Motoo, Takahashi Koji, and Ikuta Tatsuya. Experimental studies on thermal and electrical properties of platinum nanofilms. *Chinese Physics Letters*, 23(4):936, 2006.
21. B. Yang, M. Lenczner, S. Cogan, B. Gotsmann, P. Janus, and G. Boetch. Modelling, simulation and optimization for a sthm nanoprobe. In *Thermal, Mechanical and Multi-Physics Simulation and Experiments in Microelectronics and Microsystems (EuroSimE), 2014 15th International Conference on*. IEEE, 2014.
22. Qinghua Zhang. Adaptive observer for mimo linear time varying systems. 2001.